

# Insight into the nature of active species of Pt/Al<sub>2</sub>O<sub>3</sub> catalysts for low temperature NH<sub>3</sub> oxidation

Dmitry A. Svintsitskiy,<sup>[a,b]</sup> Lidiya S. Kibis,<sup>[a,b]</sup> Andrey I. Stadnichenko,<sup>[a,b]</sup> Elena M. Slavinskaya,<sup>[a,b]</sup> Anatoly V. Romanenko,<sup>[a]</sup> Elizaveta A. Fedorova,<sup>[a]</sup> Olga A. Stonkus,<sup>[a,b]</sup> Dmitry E. Doronkin,<sup>[c,d]</sup> Vasily Marchuk,<sup>[c]</sup> Anna Zimina,<sup>[c,d]</sup> Maria Casapu,<sup>[c]</sup> Jan-Dierk Grunwaldt,<sup>\*,[c,d]</sup> and Andrei I. Boronin<sup>\*,[a,b]</sup>

**Abstract:** Two series of Pt/Al<sub>2</sub>O<sub>3</sub> catalysts for low temperature NH<sub>3</sub> oxidation were prepared using Pt(NO<sub>2</sub>)<sub>4</sub> and H<sub>2</sub>PtCl<sub>6</sub> precursors. Using both precursors results in the formation of small Pt particles (d < 1.5 nm), however, Cl-containing Pt precursors give a higher fraction of highly dispersed Pt species. Such species show high stability against thermal or H<sub>2</sub> treatment probably due to the presence of substantial amount of chlorine at the surface. Treatment of the samples prepared from Pt(NO<sub>2</sub>)<sub>4</sub> with H<sub>2</sub> leads to the formation of metallic Pt nanoparticles accompanied by the improvement of catalytic activity in NH<sub>3</sub> oxidation at T < 200 °C. The main products of ammonia oxidation at temperatures below 250 °C were molecular nitrogen and nitrous oxide with the N<sub>2</sub> selectivity reaching 80%. *Operando* XANES/EXAFS revealed that even after H<sub>2</sub> pretreatment at least 40% of Pt surface remains in oxidized state under reaction conditions resulting in the appearance of N<sub>2</sub>O as a by-product.

to this, the emerging use of ammonia as an energy carrier for various mobile energy sources and transportation<sup>[11–13]</sup> also requires solving the NH<sub>3</sub> emission problem preferably via its catalytic transformation to molecular nitrogen.<sup>[14]</sup>

The catalyst for selective ammonia oxidation is an essential component of NH<sub>3</sub>-SCR diesel engine systems for NO<sub>x</sub> removal. In these systems NH<sub>3</sub> is generated onboard from aqueous urea solution.<sup>[15]</sup> For higher NO<sub>x</sub> removal efficiency excess of ammonia is dosed resulting in its slip in the exhaust. To remove NH<sub>3</sub> before it reaches the environment the Ammonia Slip Catalyst (ASC) is additionally installed.<sup>[16]</sup> The state-of-the-art ASC systems include a combination of an ammonia oxidation (AMOX) catalyst (usually, Pt/Al<sub>2</sub>O<sub>3</sub>) and a SCR catalyst in a dual-layer architecture,<sup>[15,17,18]</sup> where a part of ammonia oxidized over the Pt catalyst to N<sub>2</sub> and NO<sub>x</sub>, which is further transformed to N<sub>2</sub> over the SCR catalyst layer.

The dual-layer ASC systems have been extensively studied in the last decade. Nevertheless, there is still strong debate on full understanding of the system, which is required, for example, for the development of the kinetic models,<sup>[15]</sup> optimization of the catalyst architecture<sup>[17]</sup> and addressing catalyst deactivation.<sup>[19]</sup> In addition, further knowledge is necessary to increase the activity of AMOX catalysts to full NH<sub>3</sub> conversion below 250 °C. Among different supported noble metal catalysts, Pt-based systems are considered to be the most active for NH<sub>3</sub> oxidation.<sup>[10]</sup> However, using Pt-based catalysts requires increasing N<sub>2</sub> selectivity with minimizing the formation of undesired N<sub>2</sub>O.<sup>[20]</sup> Despite of many data about NH<sub>3</sub> oxidation to NO<sub>x</sub> over single- and polycrystalline platinum surfaces, Pt gauzes or sponges as well as supported platinum catalysts,<sup>[3,20–25]</sup> the structure-activity relationships for Pt-based systems for selective NH<sub>3</sub> oxidation to N<sub>2</sub> are still under discussion and require further systematic fundamental studies.

The ASCs operate under excess of O<sub>2</sub>, which has a great impact on the oxidation state of the active component. Over supported Pt catalysts the main issue to be considered is the relationship between the oxidation state of platinum and its particle size, as they are directly related.<sup>[26]</sup> Smaller Pt particles are readily oxidized<sup>[28,29]</sup> and the reducibility of PtO<sub>x</sub> species is found to be enhanced with the decrease of particles size.<sup>[25,30]</sup> It was proposed that metallic Pt is significantly more active for NH<sub>3</sub> oxidation than oxidized platinum,<sup>[26–28]</sup> which does not provide sites for O<sub>2</sub> dissociation.<sup>[5]</sup> Due to low resistance to oxidation small Pt nanoparticles are, therefore, considered less active in NH<sub>3</sub> oxidation than larger ones.<sup>[25,27,29]</sup> The selectivity towards various N-containing products seems to be also governed by Pt particle size and oxidation state.<sup>[22,25]</sup> The deactivation of platinum is discussed to be caused not only by the noble metal oxidation but also by accumulation of N-containing surface species especially at low temperatures.<sup>[20,30]</sup> Hence, one way to obtain efficient NH<sub>3</sub> oxidation catalysts is to carefully select the

## 1. Introduction

The strict environmental protection regulations are currently applied to control the toxic emissions from refineries, power plants and vehicles.<sup>[1,2]</sup> Exhausts of many industrial processes such as nitric acid production,<sup>[3]</sup> biomass and coal gasification,<sup>[4]</sup> the regeneration of fluid cracking catalysts (FCC),<sup>[5]</sup> and selective catalytic reduction (SCR) of NO<sub>x</sub> by NH<sub>3</sub><sup>[6]</sup> contain ammonia which has a harmful effect on human health<sup>[7,8]</sup> and environment.<sup>[9]</sup> Global NH<sub>3</sub> emission from industry was estimated to be about 220 thousand tons per year.<sup>[10]</sup> In addition

[a] Dr. D.A. Svintsitskiy, Dr. L.S. Kibis, Dr. A.I. Stadnichenko, Dr. E.M. Slavinskaya, Dr. A.V. Romanenko, E.A. Fedorova, Dr. O.A. Stonkus, Prof. Dr. A.I. Boronin  
Borokov Institute of Catalysis  
Pr. Lavrentieva 5, Novosibirsk, 630090, Russia  
E-mail: [boronin@catalysis.ru](mailto:boronin@catalysis.ru)

[b] Dr. D.A. Svintsitskiy, Dr. L.S. Kibis, Dr. A.I. Stadnichenko, Dr. E.M. Slavinskaya, Dr. O.A. Stonkus, Prof. Dr. A.I. Boronin  
Novosibirsk State University,  
Pirogova St. 2, Novosibirsk, 630090, Russia

[c] Dr. D.E. Doronkin, V. Marchuk, Dr. A. Zimina, Dr. M. Casapu, Prof. Dr. J.-D. Grunwaldt  
Institute for Chemical Technology and Polymer Chemistry  
Karlsruhe Institute of Technology (KIT),  
Engesserstr. 20, 76131, Karlsruhe, Germany  
E-Mail: [grunwaldt@kit.edu](mailto:grunwaldt@kit.edu)

[d] Dr. D.E. Doronkin, Dr. A. Zimina, Prof. Dr. J.-D. Grunwaldt  
Institute of Catalysis Research and Technology  
Karlsruhe Institute of Technology (KIT)  
Hermann-von-Helmholtz-Platz 1, 76344, Eggenstein-Leopoldshafen, Germany

Supporting information for this article is given via a link at the end of the document

Pt precursor<sup>[31,32]</sup> and the drying/pretreatment procedure<sup>[33–35]</sup>, since they can influence the size and state of Pt particles. However, the number and nature of active sites are ultimately affected by the changes in reaction conditions.<sup>[3,28,36,37]</sup> Thus, it is mandatory to establish structure-activity correlations directly during catalyst application to avoid possible modification of the active species due to the sample transfer. The rapid development of *in situ/operando* techniques, which are extensively applied in heterogeneous catalysis nowadays, can provide such an opportunity.<sup>[38–40]</sup>

This work presents a systematic study of Pt/Al<sub>2</sub>O<sub>3</sub> catalysts for low temperature NH<sub>3</sub> oxidation. The size of Pt particles and their oxidation state were varied depending on the Pt precursor and the applied calcination and/or reductive treatment. The outcome of the *operando* X-ray absorption near edge structure (XANES) study allowed us to shed light on the average oxidation state of Pt during the NH<sub>3</sub>+O<sub>2</sub> reaction. It was shown that the

improvement of catalytic properties at low temperature correlates with the Pt reduction. At higher temperature, reoxidation of Pt surface takes place leading to the NO<sub>x</sub> formation.

## 2. Results

### 2.1. Effect of the Pt precursor

#### 2.1.1. Catalytic properties

The catalytic properties of the air-calcined and reduced Pt-N-400 and Pt-Cl-400 catalysts in the NH<sub>3</sub> oxidation reaction are presented in Figure 1. Such catalysts were prepared using N- and Cl-containing Pt precursors, respectively (see *Experimental section* for details).

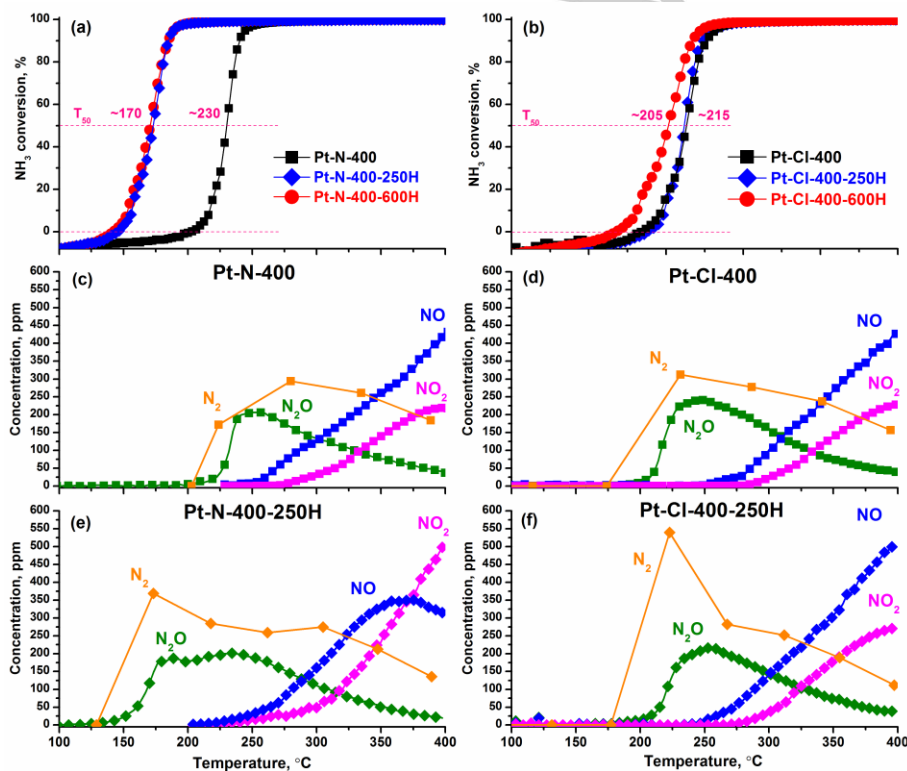


**Figure 1.** NH<sub>3</sub> conversion over (a) Pt-N-400 and (b) Pt-Cl-400 catalysts before and after reduction in H<sub>2</sub> at 250 and 600°C. Dependence of N<sub>2</sub>, N<sub>2</sub>O, NO and NO<sub>2</sub> concentrations on the reaction temperature for (c) Pt-N-400, (d) Pt-Cl-400, (e) Pt-N-400-250H, and (f) Pt-Cl-400-250H samples. The reaction mixture contains 0.1 vol.% NH<sub>3</sub> and 4.0 vol.% O<sub>2</sub> (balance He).

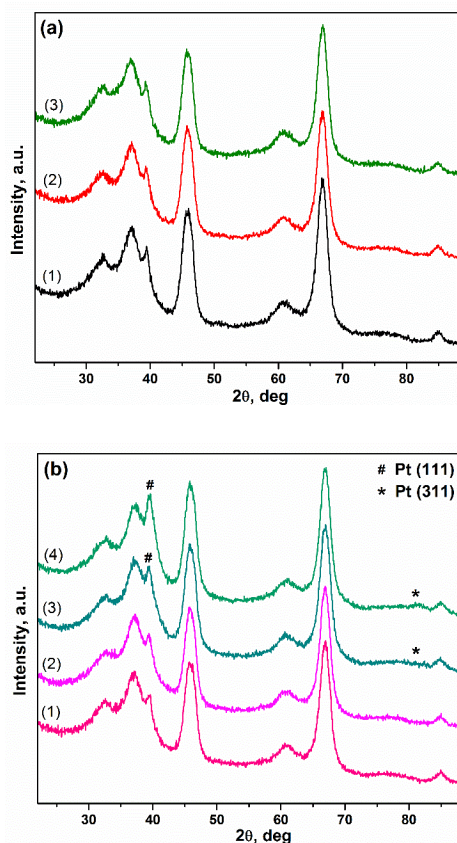


**Figure 2.** XRD data for (a) the as-prepared samples: (1)  $\gamma$ - $\text{Al}_2\text{O}_3$ , (2) *Pt-Cl-400*, (3) *Pt-N-400*; and (b) samples reduced in  $\text{H}_2$ : (1) *Pt-Cl-400-250H*, (2) *Pt-Cl-400-600H*, (3) *Pt-N-400-250H*, (4) *Pt-N-400-600H*.

All studied catalysts were characterized by the evident consumption / storage of  $\text{NH}_3$  from the reaction mixture at room temperature. It resulted in the  $\text{NH}_3$  desorption from the catalyst surface at the beginning of heating. Therefore, negative values of  $\text{NH}_3$  conversion were observed until the amount of oxidized  $\text{NH}_3$  started to exceed the amount of desorbed ammonia. In case of the *Pt-N-400* sample the temperature of 50% conversion of  $\text{NH}_3$  ( $T_{50}$ ) was ca. 230°C, while the reduction in hydrogen at 250 or 600°C caused the shift of  $\text{NH}_3$  conversion curve towards lower temperature reaching the  $T_{50}$  value of ~170°C (Figure 1a). Previously, a similar shift was also observed for  $\text{Pt}/\text{Al}_2\text{O}_3$  catalytic systems in terms of  $\text{NH}_3$  oxidation.<sup>[5,28]</sup> Note that no

significant differences in catalytic properties of the *Pt-N-400-250H* and the *Pt-N-400-600H* were observed.

Below 250°C the main products of  $\text{NH}_3$  oxidation over  $\text{Pt}/\text{Al}_2\text{O}_3$  catalysts were  $\text{N}_2$  and  $\text{N}_2\text{O}$ .  $\text{NO}$  and  $\text{NO}_2$  appeared in the effluent gas mixture only at temperatures above 250°C while the  $\text{N}_2$  and  $\text{N}_2\text{O}$  concentrations evidently decreased. This distribution of N-containing products depending on the reaction temperature is typical for the Pt-based catalysts.<sup>[41,42]</sup> The onset of  $\text{NH}_3$  conversion for all studied catalysts coincided in temperature with the simultaneous appearance of  $\text{N}_2$  and  $\text{N}_2\text{O}$ . It indicates that the same active sites were responsible for  $\text{N}_2$  and  $\text{N}_2\text{O}$  formation over  $\text{Pt}/\text{Al}_2\text{O}_3$  surface, possibly, as a result of interaction between adsorbed  $\text{N}_{\text{ads}}$  and  $\text{NO}_{\text{ads}}$  species on metallic platinum.<sup>[9,22]</sup> Reduction of the *Pt-N-400* in  $\text{H}_2$  at 250°C resulted in the clear activation of the catalyst in the temperature range from 150 to 200°C. It was accompanied by the appearance of an additional peak on the  $\text{N}_2\text{O}$  concentration curve (maximum near 180°C, Figure 1e) with simultaneous growth of  $\text{N}_2$  contribution below 200°C. Therefore, it confirms the metallic nature of sites for  $\text{N}_2/\text{N}_2\text{O}$  formation. Also, note that the  $\text{H}_2$  treatment of the *Pt-N-400* sample caused the decrease in  $\text{NO}/\text{NO}_2$  ratio above 360°C. It might be due to the change of the average Pt particle size.<sup>[25]</sup>

In case of the *Pt-Cl-400* catalyst the  $T_{50}$  value of 215°C was similar to that of the *Pt-N-400*. Reduction of the *Pt-Cl-400* in  $\text{H}_2$  at 250°C did not shift the  $\text{NH}_3$  conversion curve and only a slight decrease of the  $T_{50}$  value was observed after  $\text{H}_2$  reduction at 600°C (Figure 1b). The  $\text{N}_2$ ,  $\text{N}_2\text{O}$ ,  $\text{NO}$ , and  $\text{NO}_2$  concentration curves were rather similar to the as-prepared and reduced *Pt-Cl-400* catalysts (Figures 1d and 1f). It indicates that the  $\text{H}_2$  treatment of the *Pt-Cl-400* sample did not significantly modify its catalytic properties in contrast to the *Pt-N-400* catalyst.

#### 2.1.2. Structural characterization

X-ray diffraction (XRD) data for the *Pt-N* and *Pt-Cl* samples are given in Figure 2. The X-ray diffraction patterns of the pristine *Pt-N-400* and *Pt-Cl-400* catalysts show only reflections stemming from the of  $\gamma$ - $\text{Al}_2\text{O}_3$  phase (ICDD PDF-2 # 29-0063). (The difference curves of the X-ray patterns of the  $\text{Al}_2\text{O}_3$  support and Pt-containing samples are given in Figure S1 (cf. Supporting Information)). Reduction of the *Pt-N-400* with  $\text{H}_2$  results in appearance of small reflections from metallic Pt. Reduction at 600°C leads to the increase of the Pt particle size. The average size of  $\text{Pt}^0$  crystallites determined by the Rietveld method was 1.7 and 3.1 nm for the *Pt-N-400-250H* and *Pt-N-400-600H* samples, respectively. In case of the *Pt-Cl-400* system no reflections from  $\text{Pt}^0$  were observed in the XRD patterns even after  $\text{H}_2$  reduction at 600°C. Hence, all *Pt-Cl* samples contained platinum in a highly dispersed state.

Transmission electron microscopy (TEM) data is in a good agreement with the XRD results. The pristine *Pt-N-400* sample contains small Pt particles with average size of ~1.3 nm (Figure 3c). Reduction of *Pt-N-400* results in sintering of Pt particles with a bimodal size distribution with maxima around 1.1 and 2.1 nm (Figure 3f). Reduction at 600°C results in further increase of the particle size up to 1.5-3 nm (Figure S2). Note that the interaction of the *Pt-N* catalyst with  $\text{NH}_3+\text{O}_2$  mixture up to 400°C also resulted in a bimodal particle size distribution with maxima about

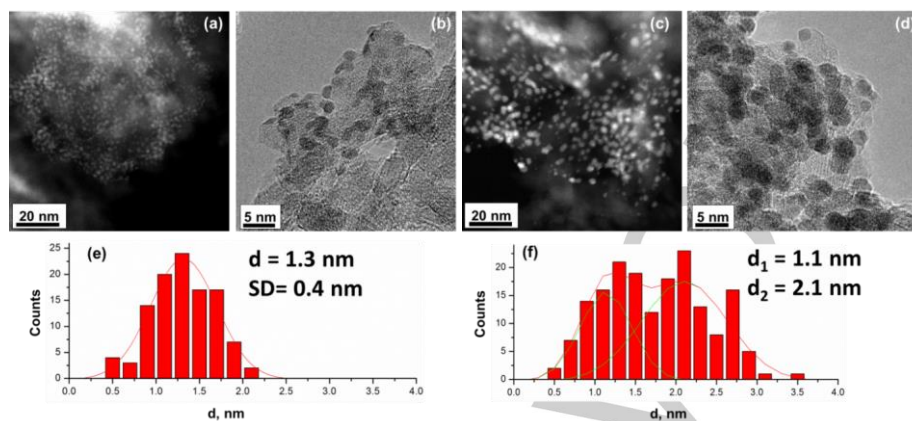


**Figure 3.** HAADF-STEM and TEM data for (a,b) *Pt-N-400* and (c,d) *Pt-N-400-250H* samples. Particle size distribution for (e) *Pt-N-400* and (f) *Pt-N-400-250H* samples with total number of particles near 100-150.

~1 and ~2 nm.<sup>[28]</sup> The *Pt-Cl-400* sample shows very small Pt particles with average size of about 0.6 nm (Figure 4). Highly dispersed Pt species can be seen as well. Treatment with H<sub>2</sub> at 250°C causes negligible increase of the average particle size up to 0.8 nm with the preservation of highly dispersed Pt species. Reduction of the sample at 600°C results in a slight increase of the average particle size up to 0.9 nm (Figure S2).

#### 2.1.3. X-ray spectroscopic investigations

Figure 5 presents X-ray photoelectron spectra (XPS) of the *Pt-N* (a) and *Pt-Cl* (b) samples. Pt4f spectra can be approximated with two doublet components. For the *Pt-N-400* sample binding energies ( $E_b$ ) of Pt4f<sub>7/2</sub> peaks are 72.2 eV and 74.3 eV. These components can be related to the oxidized species such as Pt<sup>5+</sup>/Pt<sup>2+</sup> and Pt<sup>4+</sup>, respectively.<sup>[43-45]</sup> For the *Pt-Cl-400* sample the  $E_b$ (Pt4f<sub>7/2</sub>) value for Pt<sup>4+</sup>-like component is a bit higher - 74.9 eV.

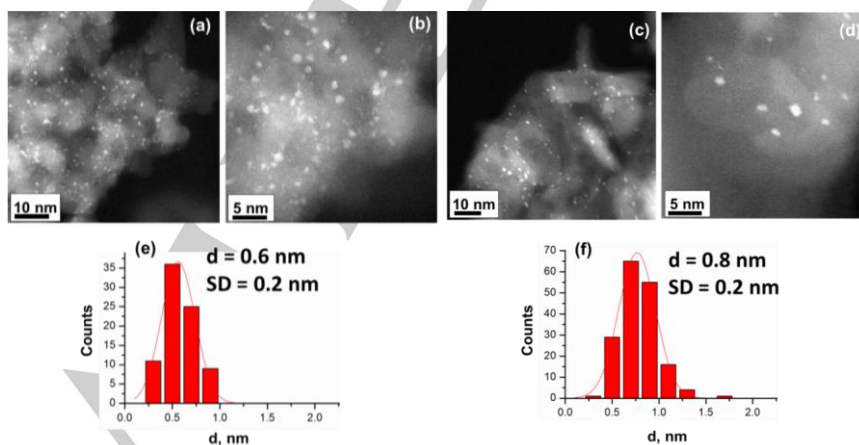


**Figure 4.** HAADF-STEM data for (a,b) *Pt-Cl-400* and (c,d) *Pt-Cl-400-250H* samples. The particle size distribution for (e) *Pt-Cl-400* and (f) *Pt-Cl-400-250H* samples with total number of particles near 100-150.

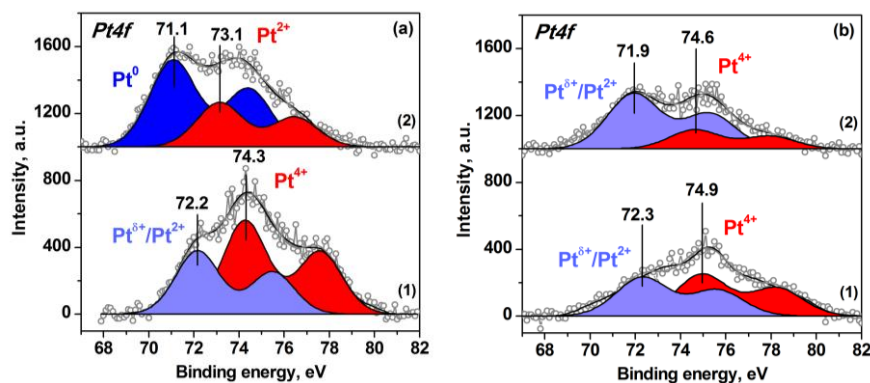


**Figure 5.** Pt4f spectra for (a) Pt-N samples: (1) Pt-N-400, (2) Pt-N-400-250H, (b) Pt-Cl samples: (1) Pt-Cl-400, (2) Pt-Cl-400-250H. Blue- and red-coloured peaks corresponds to metallic and oxidized platinum, respectively

It can be related to the presence of Cl-containing Pt compounds, including oxychlorides  $\text{PtO}_x\text{Cl}_y$ .<sup>[46]</sup> The peak at  $E_b(\text{Pt}4f_{7/2})=72.2$ - $72.3$  eV can also originate from atomically dispersed Pt species.<sup>[47]</sup> Thus, XPS points to the formation of oxidized and/or highly dispersed Pt species in the Pt-N-400 and Pt-Cl-400 samples. The spectrum of the Pt-N-400-250H sample treated with  $\text{H}_2$  shows a peak at  $E_b(\text{Pt}4f_{7/2})=71.1$  eV, typical for bulk  $\text{Pt}^0$ . A slight decrease of the ratio of Pt and Al atomic concentrations ( $\text{Pt}_{\text{at}}/\text{Al}_{\text{at}}$ ) from 1.9% to 1.6% is observed upon reduction of the Pt-N-400 sample confirming the sintering of the Pt particles (quantitative XPS data for all samples are given in Supporting Information, Table S1). The second Pt4f doublet is shifted to

lower  $E_b(\text{Pt}4f_{7/2})=73.1$  eV close to  $\text{Pt}(\text{OH})_2$  and/or PtO species.<sup>[48,49]</sup> Hence, the treatment of the Pt-N-400 sample with  $\text{H}_2$  results in substantial Pt reduction. In case of the Pt-Cl-400-250H the main Pt4f<sub>7/2</sub> peak has  $E_b(\text{Pt}4f_{7/2})$  about 71.9 eV. Increase of the binding energy compared to the value typical for bulk metallic platinum points to the formation of very small metallic ( $\text{Pt}^0$ ) or partially charged ( $\text{Pt}^{\delta+}$ ) species. The  $\text{Pt}_{\text{at}}/\text{Al}_{\text{at}}$  ratio remains about 1.1 % for the Pt-Cl-400 and the Pt-Cl-400-250H samples. Based on the XRD and TEM data, we can conclude that the  $\text{H}_2$  treatment of the Pt-Cl-400 sample results in minor reduction of Pt species without substantial increase of the particle size.

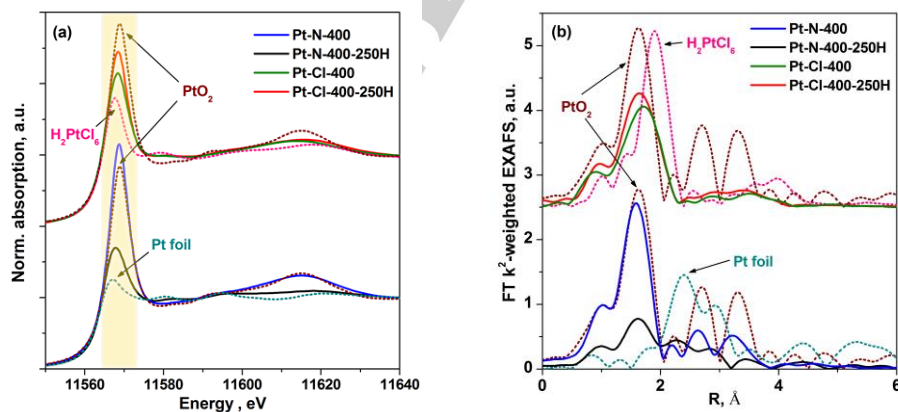


**Figure 6.** (a) Ex situ XANES (yellow field marks the "white line" peak) and (b) FT EXAFS (uncorrected for the phase shift) spectra of Pt-N-400, Pt-N-400-250H, Pt-Cl-400, Pt-Cl-400-250H, and data for  $\text{PtO}_2$ , metallic Pt and  $\text{H}_2\text{PtCl}_6$  reference samples. The k-range of EXAFS of: 2.5-10.5  $\text{\AA}^{-1}$ .

**Commented [DmDo1]:** I made a quick-and-dirty figure in GIMP, you should make it properly in Origin.



The analysis of the surface composition shows quite significant amount of chlorine in the *Pt-Cl* samples (see Table S1). Only a slight decrease of the  $\text{Cl}_{3d}/\text{Al}_{2s}$  ratio from 3.7% to 3.3% is observed upon  $\text{H}_2$  treatment of the *Pt-Cl-400* sample at 250°C. The corresponding Cl2p spectra are given in Figure S3. Based on all experimental data, the strong influence of chlorine on the tolerance of Pt species towards reduction and sintering can be reliably concluded. This conclusion is in a good agreement with the previous studies on the effect of chlorine on the properties of  $\text{Pt}/\text{Al}_2\text{O}_3$  catalysts.<sup>[32,50]</sup>

Figure 6 shows (a) XANES and (b) Fourier transformed (FT) extended X-ray absorption fine structure (EXAFS) spectra for the *Pt-N* and *Pt-Cl* samples. Intensity of the first peak above the Pt  $L_{3\alpha}$  absorption edge (so-called "white line", the region marked yellow in Figure 6a) is proportional to the density of unoccupied d-states and is often used to estimate oxidation state of  $\text{Pt}^{[51]}$  by comparing to the reference spectra for  $\text{PtO}_2$  and metallic platinum. The intensity of the white line in the *Pt-N-400* XANES spectrum is slightly higher than in the  $\text{PtO}_2$  reference spectrum which confirms fully oxidized Pt species. Reduction at 250°C leads to a significant decrease of the white line intensity in case of the *Pt-N-400-250H*. Further  $\text{H}_2$  treatment at 600°C leads to even lower white line intensity due to, possibly, sintering of Pt particles and lower availability of Pt surface for interaction with  $\text{O}_2$  from air (note that in this case the reported measurements were performed ex situ).

At the same time, the observed inconsistency between the *Pt-N-400* and  $\text{PtO}_2$  XANES spectra, probably due to the different coordination environment around Pt atoms, limits reliable quantification since  $\text{PtO}_2$  cannot be used in this case as a good reference for XANES analysis. For this reason the corresponding EXAFS spectra were also analyzed (Figure 6b).

To further evaluate the structure and quantify the average oxidation state of the Pt sites EXAFS spectra were fitted to a model containing Pt-O and Pt-Pt coordination shells from  $\text{PtO}_2$  and the first Pt-Pt coordination shell from metallic Pt (fcc). Average oxidation state of Pt is defined from an average coordination number (CN) in the Pt-O first shell (where CN=6 corresponds to  $\text{Pt}^{4+}$ ). The fitting results reported in Table 1 confirm full oxidation of the *Pt-N-400* and allow using it as a  $\text{Pt}^{4+}$  reference for linear combination analysis of XANES spectra. The FT EXAFS spectrum of *Pt-N-400-250H* allows identifying formation of Pt nanoparticles (backscattering on Pt-Pt shell at an uncorrected distance between 2 and 3 Å) while the *Pt-Cl* samples are largely oxidized and no significant Pt-Pt interaction corresponding to metallic Pt can be identified. Furthermore, both O and Cl nearest neighbors were required to achieve a good EXAFS fit of the *Pt-Cl* samples (Figure S4, Table S2). Reduction of *Pt-Cl-400* sample results in a decrease of the number of chlorine nearest neighbors and increase of oxygen backscattering.

## 2.2. Activation of Pt-Cl catalysts by high-temperature treatment

### 2.2.1. Catalytic properties

Figure 7 presents the catalytic data for  $\text{NH}_3$  oxidation over the *Pt-Cl* catalysts calcined at different temperatures, namely:

*Pt-Cl-400*, *Pt-Cl-600* and *Pt-Cl-800* catalysts. In contrast to  $\text{H}_2$  reduction at 600°C calcination in air at elevated temperature resulted in the improvement of catalytic activity accompanied by a shift of the  $\text{NH}_3$  conversion curve towards lower temperatures – to 190°C and 170°C for the *Pt-Cl-600* and *Pt-Cl-800* catalysts, respectively. In case of the *Pt-Cl-800* sample an additional peak appeared on the  $\text{N}_2\text{O}$  concentration curve in the range 150–200°C indicating the formation of additional active sites for  $\text{NH}_3$  oxidation to  $\text{N}_2/\text{N}_2\text{O}$ . It might be suggested that calcination at 800°C causes the decomposition of  $\text{PtO}_x$  species to metallic Pt particles.<sup>[52]</sup> The enhanced tolerance of such particles toward oxidation under reaction conditions is likely to be caused by their large size. The appearance of reduced/metallic Pt species was also accompanied by the increase in  $\text{NO}_2$  production at high temperatures as observed for the reduced *Pt-N-400* catalyst (Figure 1e).

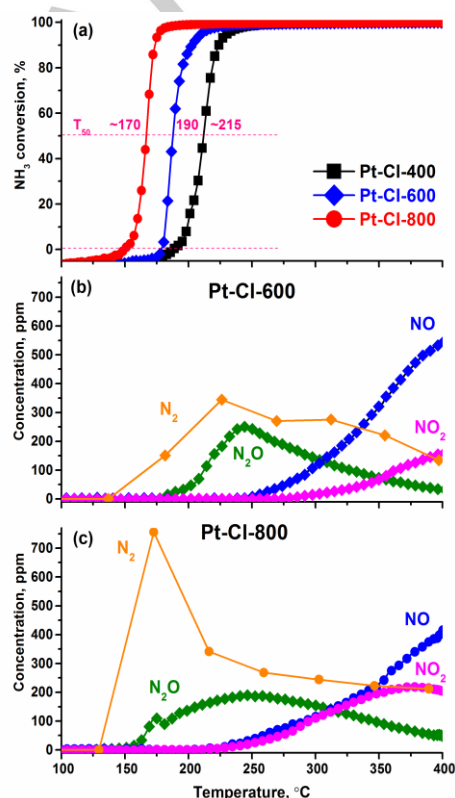


Figure 7. (a)  $\text{NH}_3$  conversion profiles over *Pt-Cl-400*, *Pt-Cl-600* and *Pt-Cl-800* catalysts. The dependence of  $\text{N}_2$ ,  $\text{N}_2\text{O}$ ,  $\text{NO}$  and  $\text{NO}_2$  concentrations on the

reaction temperature for (b) *Pt-Cl-600* and (c) *Pt-Cl-800* samples. The reaction mixture contains 0.1 vol.% NH<sub>3</sub> and 4.0 vol.% O<sub>2</sub> (balance He).

**Table 1.** A summary of average Pt oxidation states and coordination environments determined from XANES and EXAFS spectra.

Catalyst	Pt oxidation state	Pt-O (Cl)		Pt-Pt (metallic)		Pt-O (Cl)	Pt-Pt (metallic)	$\rho$ (%)
		distance (Å)	CN	distance (Å)	CN			
Pt-N-400	+4±0.7 <sup>[a]</sup>	1.99±0.01 (O)	6.0±1.0 (O)	n.a.	n.a.	2.1±2.0	9.2±1.7	0.8
Pt-N-400-250H	+1.01±0.7 <sup>[a]</sup>	1.97±0.02 (O)	1.9±0.5 (O)	2.74±0.02	6.0±2.3	4.2±4.3 (O) 9.8±3.7 (Pt)	7.0±2.1	1.6
Pt-Cl-400	-	2.00 (O) 2.27±0.06 (Cl)	3.0±0.5 (O) 2.3±3.0 (Cl)	n.a.	n.a.	7.0±10.8	10.3±5.4	4.3
Pt-Cl-400-250H	-	2.00 (O) 2.29±0.04 (Cl)	3.6±1.0 (O) 1.5±1.0 (Cl)	n.a.	n.a.	2.8±6.9	9.2±2.4	1.0

[a] determined by linear combination analysis (LCA) of XANES spectra using Pt-N-400 and Pt foil spectra as references for Pt<sup>4+</sup> and Pt<sup>0</sup> respectively in the range 11545 – 11595 eV. In lieu of Pt oxychloride reference spectra, LCA of Pt-Cl samples was not performed.

### 2.2.2. Structural characterization

XRD patterns for the *Pt-Cl* samples calcined at T≥600°C show the reflections stemming from metallic Pt (Figure 8). The average size of Pt<sup>0</sup> particles is about 18 and 50 nm for the *Pt-Cl-600* and *Pt-Cl-800* samples, respectively. Note that in case of the *Pt-Cl-600* the amount of crystalline Pt<sup>0</sup> particles is small in contrast to the *Pt-Cl-800* sample.

TEM data also show the gradual increase of the particle size with calcination of the *Pt-Cl* sample at higher temperatures (Figure 9). For the *Pt-Cl-600* sample Pt particles with size of about 0.7 nm and no highly dispersed Pt species can be detected (Figure 9c). In case of the *Pt-Cl-800* sample only large particles with size about 30-200 nm can be seen without presence of highly dispersed Pt species. Hence, calcination of the *Pt-Cl* catalyst at 600°C does not cause significant Pt sintering. The major part of platinum remains in dispersed state.

### 2.2.3. X-ray photoelectron spectroscopy

Two doublet components with E<sub>b</sub>(Pt4f<sub>7/2</sub>) at 72.1 and 74.8 eV corresponding to Pt<sup>6+</sup>/Pt<sup>2+</sup> and Pt<sup>4+</sup> species can be observed in the Pt4f spectrum of the *Pt-Cl-600* sample (Figure 10). Thus, calcination of the *Pt-Cl* sample at 600°C does not substantially change the oxidation state of platinum. Note, that the surface amount of chlorine is still high for the *Pt-Cl-600* sample reaching Cl<sub>surf</sub>/Al<sub>surf</sub> ratio of 1.9% (Figure S3). However, for the *Pt-Cl-800* sample a substantial reduction of platinum is observed. The E<sub>b</sub>(Pt4f<sub>7/2</sub>) of main peak is 71.3 eV that is close to the bulk metallic platinum, and its contribution is about 80% of the overall Pt4f signal intensity. So, air-calcination at 800°C results in substantial reduction and sintering of Pt species. However, a decrease of the Pt surface concentration is observed upon calcination at 800°C. The Pt<sub>surf</sub>/Al<sub>surf</sub> ratio decreases to ~0.5 % for the *Pt-Cl-800* sample due to the sintering of Pt particles. Also, calcination at 800°C leads to a substantial decrease of surface Cl concentration (Figure S3) indicating again the significant role of Cl for the preservation of platinum in the highly dispersed state.<sup>[32,52]</sup>

### 2.3. Operando XANES under NH<sub>3</sub>+O<sub>2</sub> conditions

In order to analyze the role of Pt state in catalytic NH<sub>3</sub> oxidation, the catalytic experiments were complemented by *operando* XANES. Figure 11 reports average oxidation state of Pt (probed in the first quarter near the inlet of the catalyst bed) as well as the simultaneously recorded catalytic data (conversion of NH<sub>3</sub> and yields of N<sub>2</sub>, N<sub>2</sub>O, and NO<sub>x</sub>) for the *Pt-N-400* and *Pt-N-400-250H* catalysts during the first and second heating in the NH<sub>3</sub>+O<sub>2</sub> mixture. Absolute error of Pt oxidation state values determined by linear combination analysis with Pt and PtO<sub>2</sub> references can reach 10% while the fits relative to the first and the last spectrum have relative error values of less than 2%, and thus the reported trends are rather precise.

When comparing the first and the second heating light-off of the *Pt-N-400* catalyst, the average oxidation state of Pt changes drastically from approx. +3.75 to less than +2. At the same time, the NH<sub>3</sub> conversion curve is only slightly (<20°C) shifted to lower temperatures and the selectivity trends are not significantly influenced.

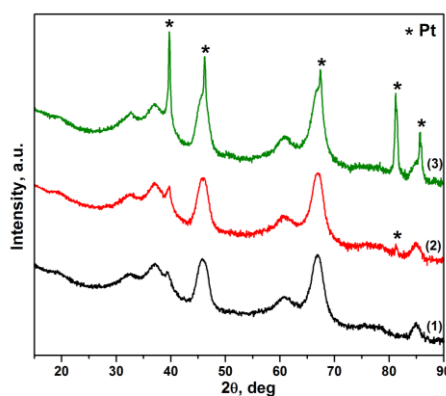


Figure 8. XRD patterns for the (1) *Pt-Cl-400*, (2) *Pt-Cl-600*, and (3) *Pt-Cl-800* samples.

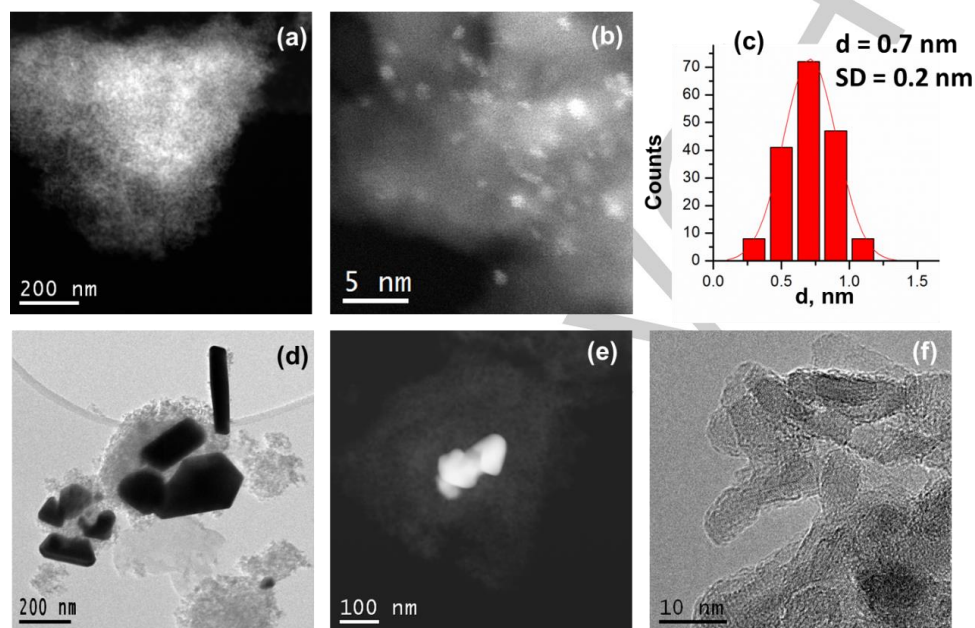


Figure 9. HAADF-STEM and HRTEM data for (a,b) *Pt-Cl-600* and (d-f) *Pt-Cl-800* samples. Particle size distribution for the (c) *Pt-Cl-600* sample with total number of particles near 150.

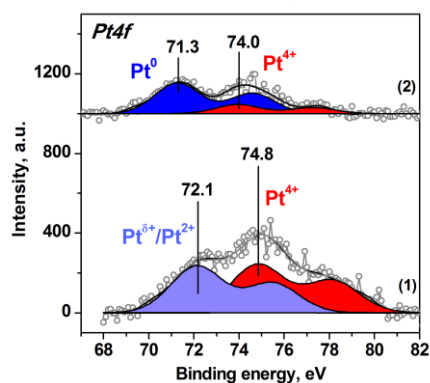


Figure 10. Pt4f spectra for (1) *Pt-Cl-600*, (2) *Pt-Cl-800* samples. Blue and red-coloured peaks correspond to metallic and oxidized platinum, respectively.

Pretreatment of the *Pt-N-400* with  $H_2$  results in a pronounced increase of  $NH_3$  conversion at temperatures below  $250^\circ C$ , in a good agreement with the catalytic data obtained in the laboratory test bench (plug flow reactor, Figure 1). The reductive pretreatment causes the decrease of the average Pt oxidation state down to +1.2 with its variation in +0.7 – +1.2 range during heating under  $NH_3+O_2$  conditions. The prereduced *Pt-N-400-250H* catalyst is characterized by Pt reduction at intermediate temperatures (corresponding to offset of  $NH_3$  conversion) and a slight increase in the Pt oxidation state at higher temperatures (Figure 11c,d). A similar but less pronounced trend is observed for the second heating of the *Pt-N-400* sample in the reaction mixture (Figure 11b). This may be a sign of surface-oxidized Pt nanoparticles being reduced by  $NH_3$  during the reaction onset with further chemisorption of oxygen at higher temperatures. Due to the high  $NH_3$  conversion at high temperature, the  $NH_3$



concentration in the gas phase is not sufficient to remove surface oxygen causing Pt oxidation. A similar behavior of Pt NPs was observed in CO oxidation.<sup>[53]</sup> The lowest value of Pt oxidation state in case of the *Pt-N-400-250H* catalyst  $\sim +0.7 - +0.8$  corresponds to the reaction temperature of 180-250°C. After this treatment  $\text{NH}_3$  conversion reaches ca. 100% and only  $\text{N}_2$  and  $\text{N}_2\text{O}$  appear as reaction products. It indicates that reduced Pt species are mainly responsible for low temperature  $\text{NH}_3$  oxidation. Furthermore, we can observe that the steady-state value of average Pt oxidation state is close to  $+0.9 \pm 0.2$ . In case of *Pt-N-400* catalyst this value was not reached during the first and the second heating-cooling cycles due to low rate of Pt oxidation/reduction.<sup>[54,55]</sup>

During the *operando* XANES study the  $\text{N}_2$ ,  $\text{N}_2\text{O}$ , and  $\text{NO}_x$  formation trends were similar for the *Pt-N-400* and *Pt-400-250H* catalysts and, hence, independent on the average oxidation state of Pt. The only difference is in the light-off temperature. Also, the  $\text{NO}_x$  contribution at high temperatures is slightly larger in case of catalyst with more reduced Pt (Figure 11c,d). This agrees well with the catalytic data obtained in the plug flow reactor (Figure 1). Hence the overall rate of  $\text{NH}_3$  oxidation is probably related to Pt oxidation state, which should be completely metallic to reach the highest catalytic activity.

However, the steady-state Pt oxidation state which can be reached in the presence of  $\text{O}_2$  excess in the reaction mixture for the NPs of 1-2 nm is only  $\sim 0.7-0.8$ . The remaining oxygen coverage on Pt surface leads to appearance of  $\text{N}_2\text{O}$  in addition to  $\text{N}_2$  at temperatures  $< 250^\circ\text{C}$ . Note that the Pt reoxidation under the reaction conditions above  $250^\circ\text{C}$  (Figure 11) is accompanied by the decrease of the selectivity towards  $\text{N}_2$  formation and increase in  $\text{NO}_x$  formation.

### 3. Discussion

Two  $\text{Pt}/\text{Al}_2\text{O}_3$  systems were thoroughly investigated by a systematic variation of the pretreatment and the combination of physicochemical techniques (XRD, XPS, *operando* XANES/EXAFS, TEM) to unravel the relationship between Pt state, particle size and catalytic properties in  $\text{NH}_3$  oxidation. The two sets of  $\text{Pt}/\text{Al}_2\text{O}_3$  catalysts were prepared by incipient wetness impregnation using  $\text{Pt}(\text{NO}_3)_4$  and  $\text{H}_2\text{PtCl}_6$  precursors.

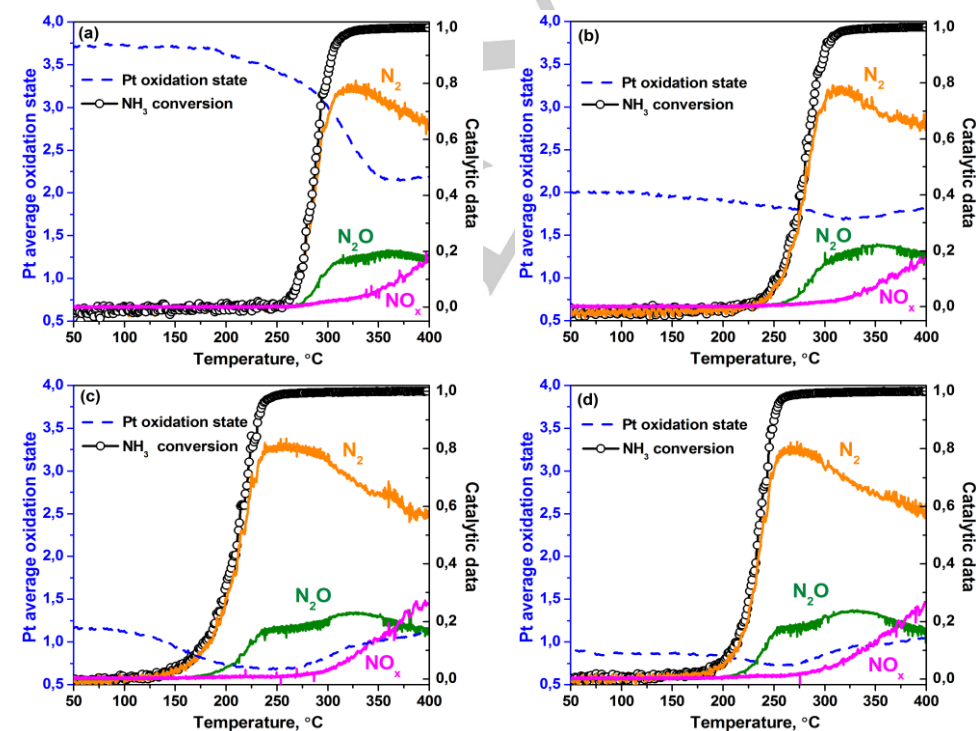


**Figure 11.**  $\text{NH}_3$  conversion,  $\text{N}_2$ ,  $\text{N}_2\text{O}$ , and  $\text{NO}_x$  yields, and Pt average oxidation state profiles obtained from *operando* XANES experiments during (a) the first and (b) second heating of Pt-N-400, and (c) the first and (d) second heating of Pt-N-400-250H. The average Pt oxidation state was determined by a linear combination analysis of the XANES spectra using internal references from QEXAFS datasets in a fitting range of 11544–11594 eV.

Calcination in air and reduction with  $\text{H}_2$  at different temperatures were applied to control the oxidation state and particle size of Pt. As-prepared  $\text{Pt}/\text{Al}_2\text{O}_3$  catalysts calcined at  $400^\circ\text{C}$  comprised of highly dispersed and deeply oxidized (Figure 5, Table 1) Pt nanoparticles with an average size less than 2 nm. Such particles exhibit significant catalytic activity in  $\text{NH}_3$  oxidation only above  $200^\circ\text{C}$  with the formation of  $\text{N}_2/\text{N}_2\text{O}$  (at  $T < 250^\circ\text{C}$ ) and  $\text{N}_2/\text{N}_2\text{O}/\text{NO}/\text{NO}_2$  (at  $T > 250^\circ\text{C}$ ) reaction products (Figure 1).  $\text{H}_2$  treatment of  $\text{Pt}/\text{Al}_2\text{O}_3$  prepared from the  $\text{Pt}(\text{NO}_3)_4$  precursor results in (1) the significant reduction of Pt (Table 1), (2) the appearance of bimodal particle size distribution with maxima at  $\sim 1$  and  $\sim 2$  nm (Figure 3), and (3) the enhancement of the  $\text{NH}_3$  oxidation activity at temperature below  $200^\circ\text{C}$ . Such an enhancement is accompanied by the evident widening of the temperature window of  $\text{N}_2/\text{N}_2\text{O}$  formation by  $50\text{--}60^\circ\text{C}$  (Figure 1). The improvement of the catalytic activity in  $\text{NH}_3$  oxidation for pre-reduced catalysts is well-known for  $\text{Ag}$ -<sup>[56,57]</sup> and Pt-based<sup>[50,58]</sup> systems owing to the generation of metallic species, which facilitate the adsorption and dissociation of  $\text{NH}_3$  in the presence of  $\text{O}_2$ .  $\text{H}_2$  treatment at high temperature ( $600^\circ\text{C}$ ) results in the increase of average Pt particle size (up to  $\sim 3$  nm) without significant changes in the catalytic properties. It indicates that Pt oxidation state is of primary importance for  $\text{NH}_3$  oxidation while the effect of Pt particle size is only related to the stabilization of metallic platinum under  $\text{O}_2$ -rich conditions.<sup>[27,28,59]</sup>

In case of  $\text{Pt}/\text{Al}_2\text{O}_3$  catalysts prepared from  $\text{H}_2\text{PtCl}_6$  precursor the treatment with  $\text{H}_2$  does not improve the catalytic activity at  $T < 200^\circ\text{C}$  due to the stabilization of highly dispersed ( $< 1$  nm, Figure 4) and oxidized Pt clusters (Table 1). It might be related to the residual Cl on the catalyst surface (Table S1). From the XPS data presented in Figure 5b, the presence of  $\text{PtO}_x\text{Cl}_y$  with  $E_b(\text{Pt}4f_{7/2}) > 74.5$  eV was revealed in the as-prepared samples as well as catalysts after the  $\text{H}_2$  treatment. Platinum oxychlorides  $\text{PtO}_x\text{Cl}_y$  interact stronger with alumina surface than  $\text{PtO}_x$  species resulting in the stabilization of highly dispersed particles.<sup>[60]</sup> Additionally, the presence of Cl might be responsible for redispersion of Pt particles at high temperatures.<sup>[32]</sup> The influence of Cl on the catalytic properties of  $\text{Pt}/\text{Al}_2\text{O}_3$  was discussed in terms of  $\text{CH}_4$  oxidation<sup>[50,60]</sup> and the decrease of catalytic activity for Cl-containing  $\text{Pt}/\text{Al}_2\text{O}_3$  catalysts was suggested to be a result of the preservation of oxidized Pt state hindering  $\text{CH}_4$  adsorption. Similarly, oxidation of Pt might have a negative effect on the adsorption of  $\text{NH}_3$ . The ammonia adsorption followed by its activation by adsorbed oxygen is considered as the rate-determining step of catalytic  $\text{NH}_3$  oxidation over platinum at low temperatures.<sup>[22,41]</sup> EXAFS data confirm the presence of Cl and O neighbors in the first coordination shell of Pt, which explains the significantly higher Pt oxidation state in the reduced  $\text{Pt}/\text{Al}_2\text{O}_3$  catalysts in contrast to Cl-free samples (Table 1). Therefore, Cl-containing  $\text{Pt}/\text{Al}_2\text{O}_3$  catalysts are not active in  $\text{NH}_3$  oxidation below  $200^\circ\text{C}$  due to the preservation of oxidized Pt species, which are unable to adsorb and activate ammonia. Only calcination at  $600\text{--}800^\circ\text{C}$  causes

removal of Cl from  $\text{Pt}/\text{Al}_2\text{O}_3$  (Table S1) resulting in the appearance of large  $\text{Pt}^0$  particles with improved catalytic activity in  $\text{NH}_3$  oxidation at  $T < 200^\circ\text{C}$  (Figure 7). Finally, the residual Cl might also influence the acidity of catalyst surface resulting in the modification of the catalytic properties.<sup>[60,61]</sup> In the present study Cl-containing and Cl-free  $\text{Pt}/\text{Al}_2\text{O}_3$  catalysts were characterized by similar amount and strength of acidic sites adsorbing  $\text{NH}_3$  at  $T > 150^\circ\text{C}$  (cf. Supporting Information), i.e. temperature at which the  $\text{NH}_3$  conversion was observed (Figures 1 and 5). Hence, it can be suggested that the modification of the surface acidity for  $\text{Pt}/\text{Al}_2\text{O}_3$  by Cl has a negligible effect on catalytic  $\text{NH}_3$  oxidation.

The treatment of the Cl-free  $\text{Pt}/\text{Al}_2\text{O}_3$  samples with  $\text{H}_2$  causes a significant enhancement of its catalytic activity in  $\text{NH}_3$  oxidation (Figure 1a) while the consequent heating-cooling cycles in  $\text{NH}_3+\text{O}_2$  mixture up to  $400^\circ\text{C}$  have little effect on its performance (Figure 11). According to the *operando* XANES data, the  $\text{H}_2$  treatment results in the decrease of average Pt oxidation state, which, then, varies between  $+0.7$  –  $+1.2$  under  $\text{NH}_3+\text{O}_2$  conditions (Figure 11). Based on the TEM, XPS and XANES data we can speculate on the ratio of metallic and oxidized Pt atoms on the surface of the *Pt-N-400-250H* sample vs. bulk species. Taking into account the Pt particle size distribution, which is the same before and after catalytic measurements,<sup>[28]</sup> the fraction of surface Pt atoms for this sample can be estimated to be  $\sim 62\%$  (cf. Supporting information). As indicated by the XPS data only  $\text{Pt}^0$  and  $\text{Pt}^{2+}$  oxidized species are present on the surface of this sample (Figure 5a). Therefore, oxidation of all surface Pt atoms ( $\sim 62\%$ ) to  $\text{Pt}^{2+}$  state would give the average Pt oxidation state  $\sim +1.25$  rather close to value initially observed for this sample by XANES (Figure 11). It indicates that interaction of pre-reduced Pt particles with oxygen leads to nearly complete oxidation of their surface, in a good agreement with previously published data.<sup>[59]</sup> During catalysis in  $\text{NH}_3+\text{O}_2$  mixture at  $T < 250^\circ\text{C}$  the decrease of the average Pt oxidation state down to  $\sim +0.7$  is observed. Note that this value might be related to the contribution of both  $\text{Pt}^{2+}$  and  $\text{Pt}^{4+}$  surface species. According to the literature data, the stoichiometry of the surface  $\text{PtO}_x$  structures upon heating in  $\text{O}_2$  depends on the Pt particle size with  $x$  value changing from 1 to 2 when particle size decreases below 2 nm.<sup>[62]</sup> Taking into account the size distribution of Pt particles for the *Pt-N-400-250H* sample we can estimate the maximal Pt oxidation state assuming that initial  $\text{Pt}^0$  nanoparticles are oxidized to  $\text{PtO}_x$  structures. The integration of the particles size distribution function with the corresponding limits (cf. Supporting Information) gives the maximal Pt oxidation state in case of *Pt-N-400-250H* catalyst close to  $\sim +2.9$ . Thus, the minimal value of Pt oxidation state observed during catalysis ( $\sim +0.7$ ) corresponds to oxidation of  $\sim 25\%$  of all Pt atoms or  $\sim 40\%$  of Pt surface. Based on the obtained results we can conclude that for the  $\text{Pt}/\text{Al}_2\text{O}_3$  samples containing 1–2 nm Pt particles at least 40% of surface Pt atoms

would be oxidized under  $\text{NH}_3$  oxidation conditions irrespective to the pretreatment procedure.

In accordance with the previously proposed mechanism of  $\text{NH}_3$  oxidation over platinum,<sup>[3,22,30]</sup> the appearance of  $\text{N}_2\text{O}$  as a reaction product is inevitable in the presence of  $\text{O}_2$  excess even at low temperatures due to high degree of Pt oxidation. It was claimed that deactivation of  $\text{Pt}/\text{Al}_2\text{O}_3$  in the catalytic  $\text{NH}_3$  oxidation occurs at temperatures below  $130^\circ\text{C}$  due to the accumulation of  $\text{NH}_x$  species on the Pt surface while adsorbed oxygen species cause deactivation at higher temperatures.<sup>[20]</sup> The presented *operando* XANES data demonstrate that in case of highly dispersed Pt particles stabilization of  $\text{PtO}_x$  species on the platinum surface takes place in the whole temperature range of interest up to  $400^\circ\text{C}$  (Figure 11). Similar behavior was established during mathematical simulations of Pt-based diesel oxidation catalysts under lean conditions.<sup>[54,63]</sup> The surface coverage of  $\text{PtO}_x$  was found to vary from 0.3 to 0.8 depending on the reaction temperature. The lowest  $\text{PtO}_x$  coverage corresponded to the highest catalytic activity which can be reached below  $200^\circ\text{C}$  due to Pt reduction or above  $400^\circ\text{C}$  as a result of  $\text{PtO}_x$  decomposition.<sup>[54]</sup> In case of  $\text{NH}_3$  oxidation the best catalytic performance is attributed to metallic Pt species providing sites for  $\text{NH}_3$  and  $\text{O}_2$  adsorption followed by ammonia activation.<sup>[5,27,41]</sup> Therefore, the degree of Pt surface oxidation should be controlled to tune the catalytic properties of Pt-based systems in  $\text{NH}_3$  oxidation including selectivity to desired reaction products.<sup>[22,25]</sup>

The most appropriate way to control Pt oxidation is a variation of Pt particle size. Larger Pt particles tend to be less oxidized while smaller  $\text{PtO}_x$  structures require higher temperatures to be reduced to  $\text{Pt}^0$ .<sup>[26,64]</sup> The optimal Pt particle size for low temperature  $\text{NH}_3$  oxidation was discussed to be in the range from 2–4 to 20 nm.<sup>[25,27]</sup> In the present work no significant difference in the  $\text{NH}_3$  oxidation rate is found for  $\text{Pt}/\text{Al}_2\text{O}_3$  catalysts with the average Pt particle size more than 2 nm (Figures 1 and 5). The highest oxidation rate is reached already for the prerduced 1–2 nm Pt particles. However,  $\text{N}_2$  selectivity for such particles does not exceed 80% (Figures 1 and 11) due to the presence of at least 40% of the oxidized Pt species on the surface under reaction conditions. To enhance the  $\text{N}_2$  selectivity the steady-state oxygen concentration on Pt surface under reaction conditions has to be decreased. Therefore, the stabilization of Pt particle size above 2 nm with narrow size distribution should be considered as a subject for further research with the aim to improve the catalytic properties of Pt-based catalysts in selective  $\text{NH}_3$  oxidation at low temperatures.

## 4. Conclusions

Platinum supported on  $\text{Al}_2\text{O}_3$  is considered as the most appropriate system for selective  $\text{NH}_3$  oxidation among various ammonia slip catalytic systems. In this work  $\text{Pt}/\text{Al}_2\text{O}_3$  catalysts prepared by impregnation using  $\text{Pt}(\text{NO}_3)_4$  and  $\text{H}_2\text{PtCl}_6$  precursors were investigated under *ex situ* and *operando* conditions to establish a relationship between Pt oxidation state,

particle size and catalytic properties in  $\text{NH}_3$  oxidation. In the presence of  $\text{O}_2$  excess in the reaction mixture the main products of  $\text{NH}_3$  oxidation were  $\text{N}_2$  and  $\text{N}_2\text{O}$  below  $250^\circ\text{C}$ , while  $\text{NO}$  and  $\text{NO}_2$  appeared at higher temperatures. It was shown that the nature of the Pt-containing precursor has a strong impact on the size of the obtained Pt nanoparticles as well as on their redox properties. The presence of residual Cl on the catalyst surface provided enhanced tolerance towards sintering and reduction of Pt during calcination and  $\text{H}_2$  treatment, respectively. The preservation of highly dispersed oxidized Pt nanoparticles due to residual Cl was proposed to be responsible for the low catalytic activity in  $\text{NH}_3$  oxidation below  $200^\circ\text{C}$ . Using a Cl-free Pt precursor during the synthesis of  $\text{Pt}/\text{Al}_2\text{O}_3$  catalysts allowed stabilizing 1–2 nm Pt particles. Reduction of such particles with  $\text{H}_2$  leads to the formation of metallic Pt species with improved catalytic activity in  $\text{NH}_3$  oxidation at  $T < 200^\circ\text{C}$ . *Operando* XANES study revealed variation of the average Pt oxidation state depending on the reaction temperature during catalytic  $\text{NH}_3$  oxidation. It was found that substantial part of Pt surface remains in oxidized form as  $\text{PtO}_x$  under  $\text{NH}_3 + \text{O}_2$  conditions at temperature below  $200^\circ\text{C}$ . It can be considered as a main reason for  $\text{N}_2\text{O}$  formation limiting the  $\text{N}_2$  selectivity to 80%. To further tune the catalytic properties of  $\text{Pt}/\text{Al}_2\text{O}_3$  catalysts in  $\text{NH}_3$  oxidation optimization of Pt particle size is required. The size of Pt particles should be large enough to prevent oxidation under reaction conditions with  $\text{O}_2$  excess, while the upper limit of Pt particles size is defined by the requirement to efficiently use the expensive active component of the catalysts.

## 5. Experimental Section

### 5.1. Sample preparation

Boehmite  $\text{AlO}(\text{OH})$  (Pural SCF-55, Sasol, Germany) was calcined in static air at  $750^\circ\text{C}$  for 4 h (heating ramp  $5^\circ/\text{min}$  with intermediate calcination at  $300^\circ\text{C}$  for 1 h) to obtain  $\gamma\text{-Al}_2\text{O}_3$  support. The specific surface area of the prepared alumina as determined by BET was  $174 \text{ m}^2/\text{g}$ . 2 wt.% Pt was deposited by incipient wetness impregnation with aqueous solutions of  $\text{Pt}(\text{NO}_3)_4$  or  $\text{H}_2\text{PtCl}_6$ . Then the samples were dried for 16 h at room temperature followed by heating to  $60^\circ\text{C}$  for 1 h and further to  $120^\circ\text{C}$  for 2 h. Finally, the catalysts were calcined in air at 400, 600 or  $800^\circ\text{C}$  for 4 h. Some samples were additionally reduced in  $\text{H}_2$  flow at 250 or  $600^\circ\text{C}$  for 2 h. Samples are designated depending on the Pt precursor (N stands for the nitrate and Cl – for chloride) and pretreatment conditions. For instance, the designation “Pt-N-400-250H” corresponds to a  $\text{Pt}/\text{Al}_2\text{O}_3$  sample prepared from  $\text{Pt}(\text{NO}_3)_4$ , calcined in air at  $400^\circ\text{C}$  followed by reduction in  $\text{H}_2$  at  $250^\circ\text{C}$ .

### 5.2. X-ray diffraction

X-ray diffraction (XRD) patterns were obtained on a Bruker D8 diffractometer (Germany) using Bragg-Brentano geometry,  $\text{CuK}_\alpha$  radiation and a Ni filter in the reflected beam path to remove the  $\text{CuK}_\beta$  component. The primary slit was  $0.1^\circ$ , the receiving one was  $2.2^\circ$ , the aperture of the Soller slits in the primary and reflected beams was  $2.5^\circ$ . The diffraction intensities were measured using an one-dimensional LynxEye detector with

an angular range of  $2.9^\circ$  on a  $2\theta$  scale. XRD patterns were collected in the  $2\theta$  range  $15\text{--}90^\circ$  with a  $0.05^\circ$  step and acquisition time of 5 s. ICDD PDF-2 powder database was used for the analysis of the crystalline phases. The structure refinement and profile analysis were carried out with the TOPAS software package.<sup>[65]</sup> The X-ray diffraction patterns for Pt/Al<sub>2</sub>O<sub>3</sub> samples were refined as a set of reflections from  $\gamma$ -Al<sub>2</sub>O<sub>3</sub> with fixed parameters (defined from a measurement of the pristine support) and metallic platinum using the Rietveld method. To estimate the instrumental broadening crystalline Si powder was used as a reference. The mean crystallite size was calculated using the LVo-IB method.<sup>[65]</sup>

### 5.3. Transmission electron microscopy

The data were collected on a JEM-2200FS electron microscope (JEOL Ltd., Japan) with an accelerating voltage of 200 kV to obtain high resolution TEM and STEM HAADF images with a spatial resolution of 1 Å. Images of crystal lattices obtained by high resolution transmission electron microscopy were analyzed by the Fourier method. The samples were dispersed in ethanol ultrasonically and deposited by sputtering the ethanol dispersion on 3 mm copper grids covered with a carbon film. The particle size distribution was determined from the TEM data using ImageJ software.<sup>[66]</sup>

### 5.4. X-ray photoelectron spectroscopy

X-ray photoelectron spectra (XPS) were measured on an ES300 spectrometer (KRATOS, UK) using MgK $\alpha$  source (1253.6 eV). The Au4f<sub>7/2</sub> and Cu2p<sub>3/2</sub> core-level spectra of gold and copper foils with binding energy ( $E_b$ ) at 84.0 eV and 932.7 eV were used for the spectrometer calibration. The maximum of the Al2p line set at 74.5 eV was used as an internal standard for calibration of the experimental spectra. Pt4f spectra were analyzed after subtraction of the Al2p signal. The Al2p, Pt4f, C1s, O1s, Cl2p core level spectra were used for analysis of surface composition and chemical state of the elements. Surface concentrations of the elements was estimated based on the intensity of the corresponding core-level spectra with consideration of atomic sensitivity factors.<sup>[67]</sup> Curve fitting was performed with a combination of Gaussian and Lorentzian functions after Shirley background subtraction. Spectra were processed using XPS-Calc program tested previously on a number of catalytic systems.<sup>[68–70]</sup>

### 5.5 X-ray absorption near edge spectra and X-ray absorption fine structure

X-ray absorption near edge structure (XANES) spectra at Pt L<sub>3</sub> absorption edge were recorded *ex situ* at the SUL-X beamline of the KIT synchrotron radiation source (Karlsruhe, Germany) in transmission mode. Catalyst samples were measured as powders packed in Kapton tubes ( $d = 1.6$  mm). The spectra were corrected for the energy shift using a spectrum of Pt foil measured simultaneously and then normalized using the Athena program from the IFFEFIT software package.<sup>[71]</sup> The average Pt oxidation state was determined from average number of oxygen atoms in the first coordination shell of Pt as obtained during analysis of extended X-ray absorption fine structure (EXAFS). For this purpose EXAFS spectra were background-subtracted,  $k^2$ -weighted and Fourier-transformed in the  $k$ -range  $2.5\text{--}10.5$  Å<sup>-1</sup> and multiplied by a Hanning window

with sill size of 1 Å<sup>-1</sup>. The amplitude reduction factor  $S_0^2=0.96$  was obtained by fitting PtO<sub>2</sub> (Alfa Aesar, 99.95%) reference spectrum to a structural model as reported in the *Inorganic Crystal Structure Database (ICSD, CC=4415)*. The fits were performed using Artemis<sup>[71]</sup> by a least square method in R-space between 1.0 and 2.5 Å in case of a single O shell and between 1.0 and 3.0 Å when fitting O and Pt (metallic) shells. Coordination numbers, interatomic distances, energy shift ( $\delta E_0$ ) and mean square deviation of interatomic distances ( $\sigma^2$ ) were refined during the fitting. The absolute misfit between theory and experiment was expressed by  $\rho$ .

For the *operando* experiments the catalysts (approx. 5 mg, pressed and sieved to 100–200  $\mu\text{m}$  grains) were placed in *in situ* microreactors (quartz capillary, 1.5 mm diameter, 20  $\mu\text{m}$  wall thickness, Hilgenberg GmbH) heated by a hot air blower.<sup>[72,73]</sup> X-rays probed the first 1 mm of catalyst near the inlet of the catalyst bed. Gases were dosed using mass flow controllers and the outlet gas was analyzed using an MKS MultiGas 2030 FTIR gas analyzer. Concentration of the produced N<sub>2</sub> was not measured directly but determined as a difference between the reacted NH<sub>3</sub> and produced NO, NO<sub>2</sub>, and N<sub>2</sub>O taking into account the number of N atoms in each of these species. The total gas flow was 70 cm<sup>3</sup>/min and the Gas Hourly Space Velocity (GHSV) – 630 000 h<sup>-1</sup>. As-prepared catalysts were heated twice in flow of 890 ppm NH<sub>3</sub> and 10 vol.% O<sub>2</sub> (He and N<sub>2</sub> mixture as balance) from 50°C to 400°C (ramp to setpoint 5°C/min, cooling down between heating in the same gas feed). Pt-N-400 and Pt-N-400-250H were measured at P64 beamline of the PETRA III synchrotron (DESY, Hamburg, Germany) operating in the QEXAFS mode. The average Pt oxidation state was determined by a linear combination analysis (LCA) of the XANES spectra using internal references from QEXAFS datasets in a fitting range of 11544–11594 eV using JAQ software.<sup>[74]</sup> To translate the relative fractions obtained from the QEXAFS analysis to the oxidation state of Pt the internal reference spectra were exported and evaluated using LCA with Pt foil and PtO<sub>2</sub> reference spectra in Athena.

### 5.6. Catalytic measurements

The catalytic measurements were carried out using an automatic setup equipped with a plug flow quartz reactor (*i.d.* = 9 mm), FTIR spectrometer (I1801, MIDAC corp., USA) and a gas chromatograph (Crystal 2000M, CHROMATEC). The catalyst weight was 0.145 g. The reaction mixture containing 0.1 vol.% NH<sub>3</sub>, 4.0 vol.% O<sub>2</sub> (balance He) was introduced at a rate of 500 cm<sup>3</sup>/min. Each sample was heated twice in the NH<sub>3</sub>+O<sub>2</sub> mixture from room temperature to 400°C at a heating rate of 10°C/min. Catalytic data obtained during the second heating in the reaction mixture are presented. Concentrations of NH<sub>3</sub>, N<sub>2</sub>O, NO and NO<sub>2</sub> were measured by gas-phase FTIR spectroscopy, while the amounts of N<sub>2</sub> and O<sub>2</sub> were defined using the gas chromatography. Ammonia conversion (in %) was calculated as  $(C_{\text{in}}-C_{\text{out}})/C_{\text{in}} \cdot 100$ , where  $C_{\text{in}}$  – inlet NH<sub>3</sub> concentration and  $C_{\text{out}}$  – outlet NH<sub>3</sub> concentration. The product selectivity ( $S_i$ ) was calculated as  $n_i/n_{\text{N}}$ , where  $n_i$  – concentration of the reaction product (N<sub>2</sub>, N<sub>2</sub>O, NO, or NO<sub>2</sub>).

### 5.7. Temperature programmed adsorption of NH<sub>3</sub> (TPD-NH<sub>3</sub>)

Before the TPD-NH<sub>3</sub> experiment, 0.25 g of each sample was outgassed in He flow at 400°C for 2 h followed by cooling to room temperature (27±2°C). Then, the sample was treated with 0.1%NH<sub>3</sub>/He mixture up to complete ammonia saturation. Afterwards the system was flushed with 500 cm<sup>3</sup>/min He flow to a residual NH<sub>3</sub> concentration below 5 ppm. Finally, the sample was heated to 400°C with a ramp rate of 10°C/min. Only NH<sub>3</sub> was detected by the combination of FTIR and GC during desorption.

### Acknowledgements

The work was supported by Helmholtz – Russian Science Foundation Joint Research Groups grant #18-43-06201 from 03.09.2018 (RSF) / HRSF-0046 from 01.09.2018 (HGF). We acknowledge DESY (Hamburg, Germany), a member of the Helmholtz Association HGF, for the provided beamtime. Parts of this research were carried out at PETRA III and we would like to thank Dr. Edmund Welter, Dr. Wolfgang Caliebe, and Dr. Vadim Murzin for assistance in using beamlines P64 and P65. We also thank the KIT synchrotron for the beamtime at SUL-X beamline and Dr. Jörg Göttlicher and Dr. Ralph Steininger for help with measurements.

**Keywords:** ammonia slip catalyst • NH<sub>3</sub> • operando • Pt/Al<sub>2</sub>O<sub>3</sub> • platinum

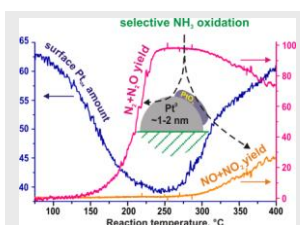
- [1] A. Walker, *Top. Catal.* **2016**, *59*, 695–707.
- [2] T. Johnson, *SAE Int. J. Engines* **2016**, *9*, 1258–1275.
- [3] R. Kraehnert, M. Baerns, *Chem. Eng. J.* **2008**, *137*, 361–375.
- [4] R. Burch, B. W. L. Southward, *J. Catal.* **2000**, *195*, 217–226.
- [5] B. Bahrami, V. G. Komvokis, M. S. Ziebarth, O. S. Alexeev, M. D. Amiridis, *Appl. Catal. B Environ.* **2013**, *130–131*, 25–35.
- [6] R. Zhang, N. Liu, Z. Lei, B. Chen, *Chem. Rev.* **2016**, *116*, 3658–3721.
- [7] H. Wu, Z. Ma, Z. Lin, H. Song, S. Yan, Y. Shi, *Nanomaterials* **2019**, *9*, 388.
- [8] A. De Marco, C. Proietti, A. Anav, L. Ciancarella, I. D'Elia, S. Fares, M. F. Fornasier, L. Fusaro, M. Gualtieri, F. Manes, et al., *Environ. Int.* **2019**, *125*, 320–333.
- [9] Y. Pan, S. Tian, D. Liu, Y. Fang, X. Zhu, Q. Zhang, B. Zheng, G. Michalski, Y. Wang, *Environ. Sci. Technol.* **2016**, *50*, 8049–8056.
- [10] L. Chmielarz, M. Jabłońska, *RSC Adv.* **2015**, *5*, 43408–43431.
- [11] D. Chakraborty, H. N. Petersen, C. Elkjær, A. Cagúlada, T. Johannessen, *Fuel Cells Bull.* **2009**, *2009*, 12–15.
- [12] S. Z. Andersen, V. Čolić, S. Yang, J. A. Schwalbe, A. C. Nielander, J. M. McEnaney, K. Eneemark-Rasmussen, J. G. Baker, A. R. Singh, B. A. Rohr, et al., *Nature* **2019**, *570*, 504–508.
- [13] Z. W. She, J. Kibsgaard, C. F. Dickens, I. Chorkendorff, J. K. Nørskov, T. F. Jaramillo, *Science* **2017**, *355*, eaad4998.
- [14] D. Chakraborty, C. D. Damsgaard, H. Silva, C. Conradsen, J. L. Olsen, H. W. P. Carvalho, B. Mutz, T. Bligaard, M. J. Hoffmann, J.-D. Grunwaldt, et al., *Angew. Chemie - Int. Ed.* **2017**, *56*, 8711–8715.
- [15] M. Colombo, I. Nova, E. Tronconi, V. Schmeißer, B. Bandl-Konrad, L. Zimmermann, *Appl. Catal. B Environ.* **2013**, *142–143*, 861–876.
- [16] K. Kamasamudram, N. Currier, M. Castagnola, H. Chen, *SAE Int. J. Engines* **2011**, *4*, 1810–1821.
- [17] S. Shrestha, M. P. Harold, K. Kamasamudram, A. Kumar, L. Olsson, K. Leistner, *Catal. Today* **2016**, *267*, 130–144.
- [18] A. Scheuer, W. Hauptmann, A. Drochner, J. Gieshoff, H. Vogel, M. Votsmeier, *Appl. Catal. B Environ.* **2012**, *111–112*, 445–455.
- [19] M. A. Smith, K. Kamasamudram, T. Szailer, A. Kumar, A. Yezerets, *SAE Tech. Pap. Ser.* **2014**, *1*, 1–6.
- [20] D. P. Sobczyk, E. J. M. Hensen, A. M. De Jong, R. A. Van Santen, *Top. Catal.* **2003**, *23*, 109–117.
- [21] W. D. Mieher, W. Ho, *Surf. Sci.* **1995**, *322*, 151–167.
- [22] E. V. Rebrov, M. H. J. M. De Croon, J. C. Schouten, *Chem. Eng. J.* **2002**, *90*, 61–76.
- [23] J. Pérez-Ramírez, E. V. Kondratenko, V. A. Kondratenko, M. Baerns, *J. Catal.* **2004**, *227*, 90–100.
- [24] A. C. M. Van Den Broek, J. Van Grondelle, R. A. Van Santen, *J. Catal.* **1999**, *185*, 297–306.
- [25] T. K. Hansen, Development of New Diesel Oxidation and NH<sub>3</sub> Slip Catalysts, Technical University of Denmark (DTU), **2017**.
- [26] A. Y. Stakheev, D. A. Bokarev, I. P. Prosvirin, V. I. Bukhtiyarov, in *Adv. Nanomater. Catal. Energy*, Elsevier Inc., **2018**, pp. 295–320.
- [27] J. J. Ostermaier, J. R. Katzer, W. H. Manogue, *J. Catal.* **1974**, *33*, 457–473.
- [28] D. A. Svintsitskiy, E. M. Slavinskaya, O. A. Stonkus, A. V. Romanenko, A. I. Stadnichenko, L. S. Kibis, E. A. Derevyannikova, A. A. Evtushkova, A. I. Boronin, *J. Struct. Chem.* **2019**, *60*, 919–931.
- [29] A. C. M. Van den Broek, Low Temperature Oxidation of Ammonia over Platinum and Iridium Catalysts, Technische Universiteit Eindhoven, **1998**.
- [30] D. P. Sobczyk, J. Van Grondelle, P. C. Thüne, I. E. Kieft, A. M. De Jong, R. A. Van Santen, *J. Catal.* **2004**, *225*, 466–478.
- [31] E. Marceau, M. Che, J. Saint-Just, J. M. Tatibouët, *Catal. Today* **1996**, *29*, 415–419.
- [32] H. Lieske, G. Lietz, H. Spindler, J. Völter, *J. Catal.* **1983**, *81*, 8–16.
- [33] O. B. Bel'skaya, R. K. Karymova, D. I. Kochubei, V. K. Duplyakin, *Kinet. Catal.* **2008**, *49*, 729–736.
- [34] R. M. Mironenko, O. B. Belskaya, V. P. Talsi, T. I. Gulyaeva, M. O. Kazakov, A. I. Nizovskii, A. V. Kalinkin, V. I. Bukhtiyarov, A. V. Lavrenov, V. A. Likholobov, *Appl. Catal. A, Gen.* **2014**, *469*, 472–482.
- [35] E. Ogel, M. Casapu, D. E. Doronkin, R. Popescu, H. Störmer, C. Mechler, G. Marzun, S. Barcikowski, M. Türk, J.-D. Grunwaldt, *J. Phys. Chem. C* **2019**, *123*, 5433–5446.
- [36] A. C. M. Van den Broek, J. Van Grondelle, R. A. Van Santen, *Catal. Letters* **1998**, *55*, 79–82.
- [37] G. Olofsson, L. R. Wallenberg, A. Andersson, *J. Catal.* **2005**, *230*, 1–13.
- [38] A. Boubnov, S. Dahl, E. Johnson, A. P. Molina, S. B. Simonsen, F. M. Cano, S. Helveg, L. J. Lemus-Yegres, J.-D. Grunwaldt, *Appl. Catal. B Environ.* **2012**, *126*, 315–325.
- [39] A. Chakrabarti, M. E. Ford, D. Gregory, R. Hu, C. J. Keturakis, S. Lwin, Y. Tang, Z. Yang, M. Zhu, M. A. Bañares, et al., *Catal. Today* **2017**, *283*, 27–53.



- [40] F. Wang, J. Jiang, B. Wang, *Catalysts* **2019**, *9*, 477.
- [41] G. Novell-Leruth, J. M. Ricart, J. Pérez-Ramírez, *J. Phys. Chem. C* **2008**, *112*, 13554–13562.
- [42] J. Schäffer, V. A. Kondratenko, N. Steinfeldt, M. Sebek, E. V. Kondratenko, *J. Catal.* **2013**, *301*, 210–216.
- [43] M. Peuchert, H. P. Bonzel, *Surf. Sci.* **1984**, *145*, 239–259.
- [44] Z. R. Ismagilov, S. A. Yashnik, A. N. Startsev, A. I. Boronin, A. I. Stadnichenko, V. V. Kriventsov, S. Kasztelan, D. Guillaume, M. Makkee, J. A. Moulijn, *Catal. Today* **2009**, *144*, 235–250.
- [45] D. A. Svintsitskiy, L. S. Kibis, A. I. Stadnichenko, S. V. Koscheev, V. I. Zaikovskii, A. I. Boronin, *ChemPhysChem* **2015**, *16*, 3318–3324.
- [46] A. V. Kalinkin, M. Y. Smirnov, A. I. Nizovskii, V. I. Bukhtiyarov, *J. Electron Spectros. Relat. Phenomena* **2010**, *177*, 15–18.
- [47] Y. T. Kim, K. Ohshima, K. Higashimine, T. Uruga, M. Takata, H. Suematsu, T. Mitani, *Angew. Chemie - Int. Ed.* **2006**, *45*, 407–411.
- [48] E. I. Vovk, A. V. Kalinkin, M. Y. Smirnov, I. O. Klembovskii, V. I. Bukhtiyarov, *J. Phys. Chem. C* **2017**, *121*, 17297–17304.
- [49] J. E. Drawdy, G. B. Hoflund, S. D. Gardner, E. Yngvadottir, D. R. Schryer, *Surf. Interface Anal.* **1990**, *16*, 369–374.
- [50] F. J. Gracia, E. E. Wolf, J. T. Miller, A. J. Kropf, *Stud. Surf. Sci. Catal.* **2001**, *139*, 471–478.
- [51] T. I. Hyde, P. W. Ash, D. A. Boyd, G. Randlishofer, K. Rothenbacher, G. Sankar, *Platin. Met. Rev.* **2011**, *55*, 233–245.
- [52] A. Boubnov, A. Gänzler, S. Conrad, M. Casapu, J.-D. Grunwaldt, *Top. Catal.* **2013**, *56*, 333–338.
- [53] A. M. Gänzler, M. Casapu, A. Boubnov, O. Müller, S. Conrad, H. Lichtenberg, R. Frahm, J.-D. Grunwaldt, *J. Catal.* **2015**, *328*, 216–224.
- [54] A. Arvajová, P. Kočí, *Chem. Eng. Sci.* **2017**, *158*, 181–187.
- [55] L. Olsson, H. Karlsson, *Catal. Today* **2009**, *147*, 12–15.
- [56] L. Zhang, H. He, *J. Catal.* **2009**, *268*, 18–25.
- [57] L. Gang, B. G. Anderson, J. Van Grondelle, R. A. Van Santen, *Appl. Catal. B Environ.* **2003**, *40*, 101–110.
- [58] D. P. Sobczyk, A. M. De Jong, E. J. M. Hensen, R. A. Van Santen, *J. Catal.* **2003**, *219*, 156–166.
- [59] R. W. McCabe, C. Wong, H. S. Woo, *J. Catal.* **1988**, *114*, 354–367.
- [60] E. Marceau, H. Lauron-Pernot, M. Che, *J. Catal.* **2001**, *197*, 394–405.
- [61] P. Berteau, B. Delmon, *Catal. Today* **1989**, *5*, 121–137.
- [62] C.-B. Wang, C.-T. Yeh, *J. Catal.* **1998**, *178*, 450.
- [63] A. Arvajová, P. Kočí, V. Schmeißer, M. Weibel, *Appl. Catal. B Environ.* **2016**, *181*, 644–650.
- [64] N. Seriani, Z. Jin, W. Pompe, L. C. Ciacchi, *Phys. Rev. B - Condens. Matter Mater. Phys.* **2007**, *76*, 1–10.
- [65] TOPAS, version 4.2., Bruker AXS Inc., 2009, Madison, Wisconsin, USA n.d.
- [66] M. D. Abramoff, P. J. Magalhaes, J. S. Ram, *Biophotonics Int.* **2004**, *11*, 36–42.
- [67] J. F. Moulder, W. F. Stickle, P. E. Sobol, K. D. Bomben, *Handbook of X-Ray Photoelectron Spectroscopy*, Perkin-Elmer Corp, Eden Prairie, Minnesota, USA, **1992**.
- [68] L. S. Kibis, D. A. Svintsitskiy, T. Y. Kardash, E. M. Slavinskaya, E. Y. Gotovtseva, V. A. Svetlichnyi, A. I. Boronin, *Appl. Catal. A Gen.* **2019**, *570*, 51–61.
- [69] E. D. Grayfer, L. S. Kibis, A. I. Stadnichenko, O. Y. Vilkov, A. I. Boronin, E. M. Slavinskaya, O. A. Stonkus, V. E. Fedorov, *Carbon N. Y.* **2015**, *89*, 290–299.
- [70] D. A. Svintsitskiy, E. M. Slavinskaya, T. Y. Kardash, V. I. Avdeev, B. V. Senkovskiy, S. V. Koscheev, A. I. Boronin, *Appl. Catal. A Gen.* **2016**, *510*, 64–73.
- [71] B. Ravel, M. Newville, *J. Synchrotron Radiat.* **2005**, *12*, 537–541.
- [72] J.-D. Grunwaldt, N. Van Vegten, A. Baiker, *Chem. Commun.* **2007**, 4635–4637.
- [73] D. E. Doronkin, H. Lichtenberg, J.-D. Grunwaldt, in *XAFS Tech. Catal. Nanomater. Surfaces*, **2016**, pp. 75–89.
- [74] B. Bornmann, J. Kläs, O. Müller, D. Lützenkirchen-Hecht, R. Frahm, *AIP Conf. Proc.* **2019**, *2054*, 40008.

## FULL PAPER

**Ammonia shall not pass:** Metallic Pt is the most active in  $\text{NH}_3$  oxidation at  $T < 200^\circ\text{C}$ . Surface of Pt nanoparticles is found to be oxidized under  $\text{NH}_3 + \text{O}_2$  conditions. It results in the formation of undesirable products. The presence of Cl on catalyst surface hinders platinum reduction decreasing catalyst activity.



Dr. Dmitry A. Svintsitskiy, Dr. Lidiya S. Kibis, Dr. Andrey I. Stadnichenko, Dr. Elena M. Slavinskaya, Dr. Anatoly V. Romanenko, Elizaveta A. Fedorova, Dr. Olga A. Stonkus, Dr. Dmitry E. Doronkin, Vasyi Marchuk, Dr. Anna Zimina, Dr. Maria Casapu, Prof. Jan-Dierk Grunwaldt,\* Prof. Andrei I. Boronin\*

Page No. – Page No.

Insight into the nature of active species of  $\text{Pt}/\text{Al}_2\text{O}_3$  catalysts for low temperature  $\text{NH}_3$  oxidation